JOURNAL OF THEORETICAL AND APPLIED MECHANICS
62, 3, pp. 507-519, Warsaw 2024
https://doi.org/10.15632/jtam-pl/188526

DETERMINATION OF CHABOCHE AND BOUC-WEN PARAMETERS FOR QUENCHED AND TEMPERED STEEL

Ciro Santus, Lorenzo Romanelli, Tommaso Grossi, Paolo Neri
University of Pisa, Department of Civil and Industrial Engineering (DICI), Pisa, Italy
e-mail: ciro.santus@unipi.it; lorenzo.romanelli@phd.unipi.it (corresponding author);
tommaso.grossi@phd.unipi.it; paolo.neri@unipi.it

During cyclic loadings, metal alloys can undergo cyclic plasticity, for example, at notches. The Chaboche kinematic hardening model provides a versatile and realistic description of the material stress-strain behaviour under multiaxial cyclic loadings. In this work, the global properties, extracted from stabilized cycles of strain-controlled tests and from a force--controlled test, are employed to calculate the parameters. Alternatively, the Bouc-Wen model can provide a reliable representation of nonlinear hysteretic phenomena, and the classic nonlinear least squares approach is employed to tune its constants. The performances of the two proposed techniques are compared, and a final discussion is provided.

Keywords: cyclic-plasticity, hysteretic behaviour, Chaboche kinematic hardening model, Bouc-Wen model

1. Introduction

The presence of notches in mechanical components can enhance the plastic behaviour, in particular, under cyclic loadings, thus an accurate description of the constitutive behaviour of metal alloys is crucial for structural analysis. For example, in (Bertini *et al.*, 2017; Santus *et al.*, 2023b) the use of a cyclic plastic constitutive law was motivated by the fact that, assuming purely elastic behaviour, the presence of a severe V-notch combined with a high fatigue load ratio R ($R = \sigma_{min}/\sigma_{max}$), resulted in very high and not meaningful values of stress near the notch. The Chaboche kinematic hardening (CKH) model (Chaboche, 1986) is a powerful and recognized model to describe the cyclic plastic behaviour of metals. Given that it is a kinematic model, it accounts for the Bauschinger effect, which generally occurs during the cyclic plastic behaviour of materials. This latter statement, together with the necessity to consider the plastic behaviour of the material near the notches, justifies the widespread use of this model in fatigue analyses such as in (Karolczuk *et al.*, 2019; Hosseini and Seifi, 2020; Santus *et al.*, 2022). The CKH model is also implemented in Ansys finite element (FE) software.

Since its first introduction, the Chaboche model has undergone several proposals of modification. Chaboche himself (Chaboche, 1991) suggested a modification to improve the ratcheting prediction, which was subsequently validated by other researchers (Shafiqul and Tasnim, 2000). Some changes to the classical CKH model were also proposed by (Dafalias *et al.*, 2008), where the parameters of backstress components were assumed variable during cyclic-loading to improve the ratcheting rate prediction. Despite all the modifications of the Chaboche hardening rule, the computation of Chaboche parameters is a challenging task even considering the classical formulation of this model. Typically, only stabilized cycles extracted from strain-controlled tests (SCTs) on plain specimens can be used to calculate the parameters, but force-controlled tests (FCT) can also be used as in (Koo and Lee, 2007; Mahmoudi *et al.*, 2011). Different techniques can be employed to obtain the Chaboche parameters such as genetic algorithms (Badnava *et al.*,

2012; Dvoršek *et al.*, 2023), particle-swarm optimization (Li *et al.*, 2018) and gradient-based optimization algorithm (Chaparro *et al.*, 2008). The latter algorithms typically demand substantial computational resources.

Alternatively, the Bouc-Wen (B-W) model (Bouc, 1967; Wen, 1976) is widely employed to describe the hysteretic behaviour of mechanical systems such as piezo-actuated devices (Cai *et al.*, 2023) or wire rope isolators (Neri and Holzbauer, 2023). Various optimization algorithms can be again employed to obtain B-W parameters such as the Levenberg-Marquardt algorithm (Ni *et al.*, 1998), multi-objective optimization algorithms (Ortiz *et al.*, 2013) or particle-swarm optimization (Charalampakis and Dimou, 2010).

In this research, a novel and physics-based algorithm to calculate the CKH model parameters was employed. The global properties of stabilized cycles of the SCTs, such as the gradient at extreme points of the cycles (EPOC), the hysteresis area (HA), the stress range (SR), the average stress (AS), the average plastic strain (APS) and the plastic strain range (PSR) were employed to compute the parameters. To provide an accurate description of the transient during the FCT, the experimental ratcheting rate was also employed during determination of the parameters. The Bouc-Wen model was also used to replicate the cyclic-plastic behaviour considering the nonlinear hysteretic nature of cyclic plastic phenomena. However, the search of the parameters required a different strategy due to different nature of model equations.

Section 2 is dedicated to show the experimental data and, in Section 3, the utilized procedure to calculate the CKH parameters is explained along with the corresponding obtained results. In Section 4, the Bouc-Wen model is introduced and the corresponding results to model the cyclic plastic behaviour are shown. Finally, in Section 5, a discussion with a comparison between the two engaged algorithms is provided.

2. Materials

The alloy investigated in this research is 42CrMo4 quenched and tempered steel. All tests were performed on plain specimens (i.e. without notches) and under uniaxial loading. The mean values of the yield strength and of the ultimate strength, obtained by a standard tensile test, were equal to $S_Y = 500\,\text{MPa}$ and $S_U = 700\,\text{MPa}$, respectively. Three SCTs and one FCT were employed to calculate the CKH parameters. Two SCTs were performed at $R_\varepsilon = -1$, which means that the minimum imposed total axial strain and the maximum imposed total axial strain were opposite, while one was performed at $R_\varepsilon \neq -1$. The FCT was conducted at $R = -0.66$, and R indicates the ratio between the minimum and the maximum imposed axial stress. The SCTs conducted at $R_\varepsilon = -1$ are shown in Fig. 1, Cycle I (C_I) and Cycle II (C_{II}) indicate the stabilized cycles and ε_p represents the axial plastic strain. The useful quantities extracted from the stabilised cycles are also shown in Fig. 1, and their corresponding numerical values are reported in Table 1.

Table 1. Global properties extracted from C_I and C_{II}

	$\Delta\varepsilon_p$ [–]	$\Delta\sigma$ [MPa]	A [mJ/mm^3]	$d\sigma/d\varepsilon_p$ [GPa]
C_I	1.43%	1030	12.0	5.81
C_{II}	0.50%	918	3.61	20.2

The useful quantities extracted from the FCT in order to apply the procedure are shown in Fig. 2. The ratcheting rate in Fig. 2b presents an initial linear trend, which is used to calculate the Chaboche parameters. It is important to remark that the CKH model is not able to reproduce a variable (increasing) ratcheting rate, unless combining the CKH model with damage mechanics models.

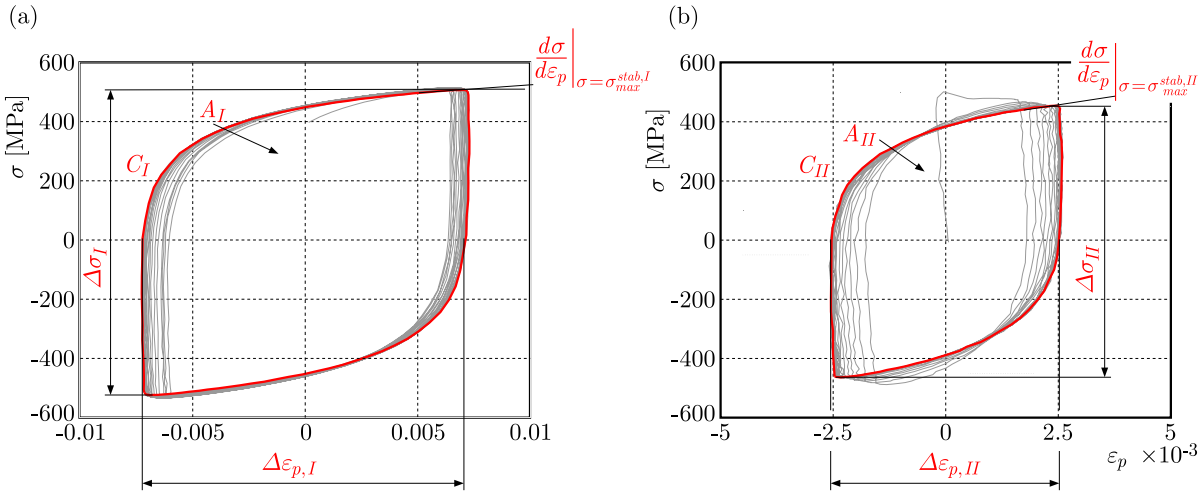

Fig. 1. Strain-controlled tests performed at $R_\varepsilon = -1$, the transient cycles are indicated in grey, while the stabilized cycles are marked in red as (a) C_I and (b) C_{II}

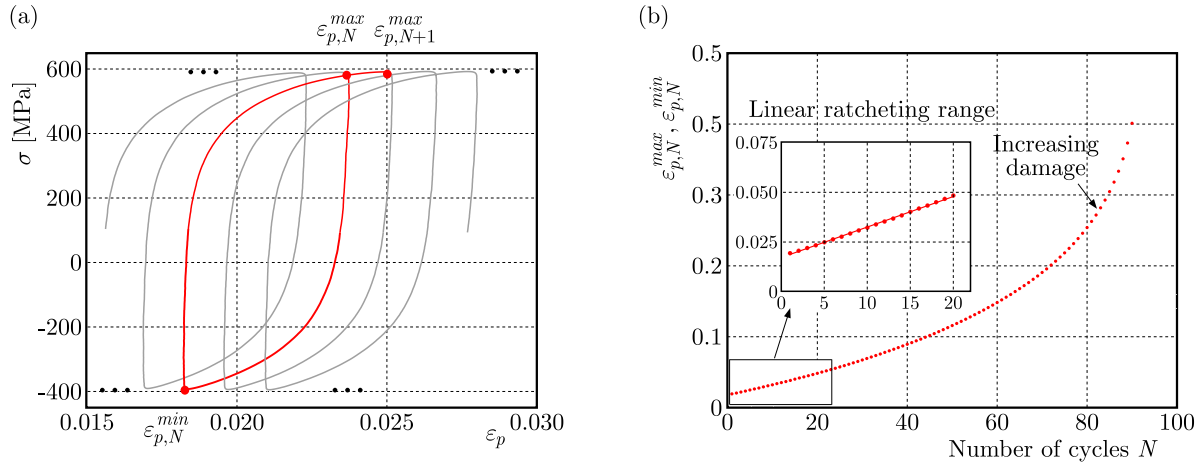

Fig. 2. (a) Few cycles of the force-controlled test involved in the research with significant quantities highlighted; (b) experimental maximum plastic strain per cycle of the force-controlled test employed in this research

From Fig. 2a some useful quantities need to be defined as the plastic strain amplitude (PSA) per cycle and the plastic strain rate per cycle, which are formalized as

$$\Delta\varepsilon^a_{p,N} = \frac{\varepsilon^{max}_{p,N+1} + \varepsilon^{max}_{p,N}}{2} - \varepsilon^{min}_{p,N} \qquad \Delta\varepsilon^r_{p,N} = \varepsilon^{max}_{p,N+1} - \varepsilon^{max}_{p,N} \tag{2.1}$$

These two quantities $\Delta\varepsilon^a_{p,N}$ and $\Delta\varepsilon^r_{p,N}$ are not generally constant. However, FE simulations by involving the Chaboche model showed that, after the initial cycles, a constant ratcheting rate can be obtained as described in (Kreethi *et al.*, 2017; Zhang *et al.*, 2020). Given these latter findings, the two quantities of Eqs. (2.1) can be assumed constant in order to describe the ratcheting rate, and they can be substituted with $\Delta\varepsilon^a_p$ and $\Delta\varepsilon^r_p$ in which there is no dependence on the number of cycles N.

3. Computation of the CKH parameters

For a plain specimen loaded uniaxially, and employing the CKH model, the dependence between the axial stress σ and the backstress components can be described by Eqs. (3.1). In these

equations σ_L is the elastic limit (to be calculated), μ is a coefficient equal to 1 during positive loading ramps, and to -1 during negative loading ramps and χ is the total backstress obtained by the sum of backstress components

$$\sigma = \mu\sigma_L + \chi \qquad \chi = \sum_{i=1}^{n} \chi_i \qquad d\chi_i = C_i d\varepsilon_p - \gamma_i \chi_i |d\varepsilon_p| \tag{3.1}$$

The third of Eqs. (3.1) describes a differential equation which governs the dynamics of the backstress components. C_i and γ_i are the CKH model parameters to be tuned. In this work, the classical CKH model with three backstress components was calibrated, and the fourth backstress was eventually added to improve the prediction of stabilized cycles of the SCTs near the elastic limit zones. The qualitative trends of the three backstress components, according to our procedure and for an ideal plastic strain controlled test with $R_{\varepsilon p} = 0.1$, are reported in Fig. 3. The first backstress has the most rapid dynamics (Fig. 3a), while the second backstress has much slower dynamics than that of the first one (Fig. 3b). Finally, the third backstress was assumed with a linear trend as shown in Fig. 3c that is just obtained by imposing $\gamma_3 = 0$. It is important to highlight that the first backstress leads to a nonzero value of the HA of the stabilized cycle, while the second backstress leads to an almost null value of the HA of the stabilized cycle, which can be approximated as null in the following analysis. The maximum and the minimum values of the first and second backstress components, as concerns the stabilized cycles, are opposite as highlighted in Figs. 3b and 3c. On the contrary, a nonzero mean stress remains for the linear backstress component, despite the loading cycling.

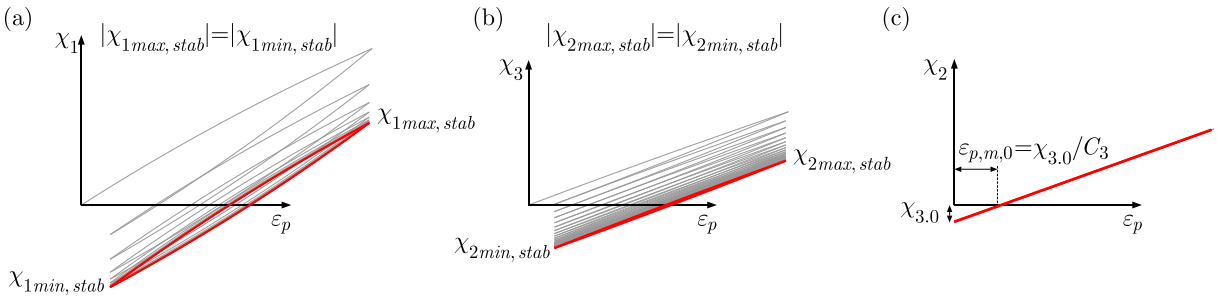

Fig. 3. Trends of the three backstress components for ideal plastic SCT at $R_{\varepsilon p} = 0.1$: (a) first backstress component (fast), (b) second backstress component (slow) and (c) third backstress component (stable)

The CKH parameters to be determined were C_1, γ_1, C_2, γ_2, C_3, $\chi_{3,0}$ and σ_L, and the procedure to calculate them was presented in (Santus *et al.*, 2023a) and is briefly recalled here. Using the average point of the stabilized cycles extracted from the SCTs, the parameters C_3 and $\chi_{3,0}$ were determined by combining C_I and Cycle III (C_{III}), which indicates the stabilized cycle of the strain-controlled test (SCT) performed at $R_\varepsilon \neq -1$. Equations (3.2) provide a 2×2 linear system which relates the AS $\sigma_m = (\sigma_{max} + \sigma_{min})/2$ and the APS $\varepsilon_{p,m} = (\varepsilon_{p,max} + \varepsilon_{p,min})/2$ of the stabilized cycles, which are also the experimental inputs. When the experimental SCT performed at $R_\varepsilon \neq -1$ is almost fully relaxed, the obtained value of C_3 is much lower than the values of C_1 and C_2

$$\chi_{3,0} + C_3 \varepsilon_{p,m,I} = \sigma_{m,I} \qquad \chi_{3,0} + C_3 \varepsilon_{p,m,II} = \sigma_{m,II} \tag{3.2}$$

Once the parameters C_3 and $\chi_{3,0}$ were calculated, Eqs. (3.3)-(3.5) were employed to calculate the other parameters, except for γ_2, which was calculated using the FCT. The experimental inputs of Eqs. (3.3)-(3.5) were all extracted from the stabilized cycles of the SCTs performed at $R_\varepsilon = -1$ (C_I and C_{II}). Assuming the inequality given by $\gamma_2 \Delta\varepsilon_p \ll 1$, which is meaningful considering the low value of γ_2 and which was employed in all the following equations, Eqs. (3.3)

can be obtained to model the gradient at the EPOC in the $\sigma - \varepsilon_{pl}$ plane. In Eqs. (3.3), the PSR $\Delta\varepsilon_p = (\varepsilon_{p,max} - \varepsilon_{p,min})$ and the gradient at the EPOC, $d\sigma/d\varepsilon_p$ calculated at σ_{max}^{stab}, are the experimental inputs, and the nonlinear system can be solved to obtain the expressions for C_1 and C_2 depending on γ_1

$$\begin{aligned} C_1\Big(1 - \tanh\frac{\gamma_1\Delta\varepsilon_{p,I}}{2}\Big) + C_2 &= -C_3 + \left.\frac{d\sigma}{d\varepsilon_p}\right|_{\sigma=\sigma_{max}^{stab,I}} \\ C_1\Big(1 - \tanh(\frac{\gamma_1\Delta\varepsilon_{p,II}}{2}\Big) + C_2 &= -C_3 + \left.\frac{d\sigma}{d\varepsilon_p}\right|_{\sigma=\sigma_{max}^{stab,II}} \end{aligned} \tag{3.3}$$

The expressions to calculate the values of the elastic limit for C_I and C_{II} were obtained as functions depending on γ_1 only, as shown in Eqs. (3.4). In these latter equations, the PSR and the SR $\Delta\sigma = (\sigma_{max} - \sigma_{min})$ are, in turn, the experimental inputs. The expressions of $\sigma_{L,I}$ and $\sigma_{L,II}$ obtained from Eqs. (3.4) should lead to the same value considering that the elastic limit is obviously a unique material property. Given that this assumption is not satisfied, in general, an averaged function was defined as $\sigma_L = (\sigma_{L,I} + \sigma_{L,II})/2$

$$\begin{aligned} \sigma_{L,I} &= \frac{\Delta\sigma_I}{2} - \frac{C_1}{\gamma_1}\tanh\frac{\gamma_1\Delta\varepsilon_{p,I}}{2} - \frac{C_2 + C_3}{2}\Delta\varepsilon_{p,I} \\ \sigma_{L,II} &= \frac{\Delta\sigma_{II}}{2} - \frac{C_1}{\gamma_1}\tanh\frac{\gamma_1\Delta\varepsilon_{p,II}}{2} - \frac{C_2 + C_3}{2}\Delta\varepsilon_{p,II} \end{aligned} \tag{3.4}$$

The last property to be considered during the determination of the parameters is the HA of the stabilized cycle, which is described for C_I and C_{II}, by A_I^{mod} and A_{II}^{mod}, respectively. It is important to highlight that Eqs. (3.2)-(3.5) were obtained in (Santus *et al.*, 2023a) by supposing plastic SCTs, but they were extended to total SCTs without any loss of generality

$$\begin{aligned} A_I^{mod} &= 2\sigma_L\Delta\varepsilon_{p,I} + 2\Big(\frac{C_1}{\gamma_1}\Delta\varepsilon_{p.I} - 2\frac{C_1}{\gamma_1^2}\tanh\frac{\gamma_1\Delta\varepsilon_{p,I}}{2}\Big) \\ A_{II}^{mod} &= 2\sigma_L\Delta\varepsilon_{p,II} + 2\Big(\frac{C_1}{\gamma_1}\Delta\varepsilon_{p.II} - 2\frac{C_1}{\gamma_1^2}\tanh\frac{\gamma_1\Delta\varepsilon_{p,II}}{2}\Big) \end{aligned} \tag{3.5}$$

Three error functions, all depending on γ_1 only, were then defined:

- An error function to quantify the difference between the values obtained by the expression of $\sigma_{L,I}$ and those obtained by the expression of $\sigma_{L,II}$

$$\Sigma = \Big|\frac{\sigma_{L,I} - \sigma_{L,II}}{\sigma_L}\Big|$$

- A relative error function about the HA of C_I

$$\Lambda_I = \frac{A_I^{mod} - A_I}{A_I}$$

- A relative error function about the HA of C_{II}

$$\Lambda_{II} = \frac{A_{II}^{mod} - A_{II}}{A_{II}}$$

The three introduced error functions were then included into a global error function, which is presented in

$$\psi(\gamma_1) = (1 - \alpha)\Sigma^2 + \alpha(\Lambda_I^2 + \Lambda_{II}^2) \tag{3.6}$$

The weight parameter α can balance between the importance of considering the relative error of the HA and the error about the cycle amplitude. The parameter α is considered in the range $[0,1]$. The searched value of γ_1 was just found by minimizing the global error function presented in Eq. (3.6). A qualitative trend of the global error function $\psi(\gamma_1)$, obtained with $\alpha = 0.5$, is shown in Fig. 4. Once the value of γ_1 was obtained, the parameters C_1, C_2 and σ_L were then easily numerically calculated by following the expression proposed in Eqs. (3.3)-(3.5). The last parameter to be calculated was γ_2 by involving the FCT. Considering the CKH model with only two nonlinear backstress components, the relationship between the AS, the PSA per cycle and the plastic strain rate per cycle for a FCT on a plain specimen is provided by

$$\sigma_m = \sum_{i=1}^{2} \frac{C_i}{\gamma_i} \frac{\sinh(\gamma_i \Delta\varepsilon_p^r/2)}{\sinh(\gamma_i \Delta\varepsilon_p^a)} \tag{3.7}$$

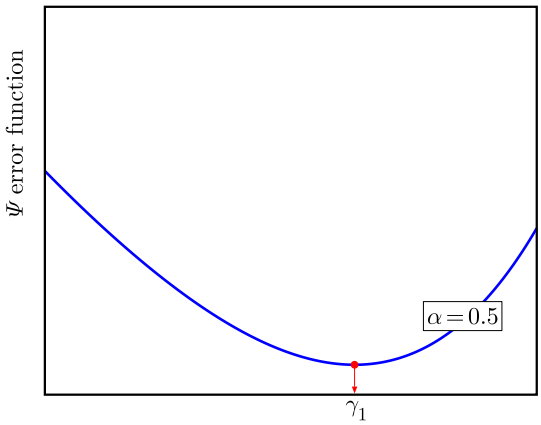

Fig. 4. An example of the trend of the global error function $\psi(\gamma_1)$ with $\alpha = 0.5$

Considering that, generally, $\gamma_i \Delta\varepsilon_p^r \ll 1$ for each backstress component giving a small plastic strain increment per cycle, Eq. (3.7) can be simplified into Eq. (3.8). This latter equation can be easily inverted, and the value of γ_2 can thus be obtained

$$\sigma_m = \sum_{i=1}^{2} \frac{C_i}{\sinh(\gamma_i \Delta\varepsilon_p^a)} \tag{3.8}$$

When the third linear backstress is also considered, the maximum value of this backstress component evolves cycle per cycle according to

$$\chi_{3,i+1}^{max} = \chi_{3,i}^{max} + C_3 \Delta\varepsilon_p^r \tag{3.9}$$

This latter equation highlights that the only achievable equilibrium, when the third linear backstress component is considered, occurs for $\Delta\varepsilon_p^r = 0$, i.e. for a plastic shakedown. According to this latter statement, the quantities $\Delta\varepsilon_{p,N}^a$ and $\Delta\varepsilon_{p,N}^r$ cannot be considered constant. The relationships shown by Eqs. (3.2), which were used for SCTs, are also valid to describe the average point of the stabilized cycle of a FCT as remarked in (Santus, Grossi *et al.*, 2023). Therefore, the relationship to describe the APS of the stabilized cycle can be obtained by inverting Eqs. (3.2), thus obtaining

$$\varepsilon_{p,m} = \frac{\sigma_m - \chi_{3,0}}{C_3} \tag{3.10}$$

This equation highlights that the APS of the stabilized cycle of a FCT is relatively high for low values of C_3, thus it is reached after a quite big number of cycles. Therefore, the PSA per cycle

and the plastic strain rate per cycle can be considered constant without any loss of accuracy, and Eq. (3.8) can be finally employed to obtain the value of γ_2. In Fig. 5, some of the obtained results are reported, more specifically, in Fig. 5a, the blue line predicts the mean points of the stabilized cycles as described in Eqs. (3.2), and in Fig. 5b, differences between the experimental stabilized cycles C_I and C_{II} and the corresponding modelled cycles are shown.

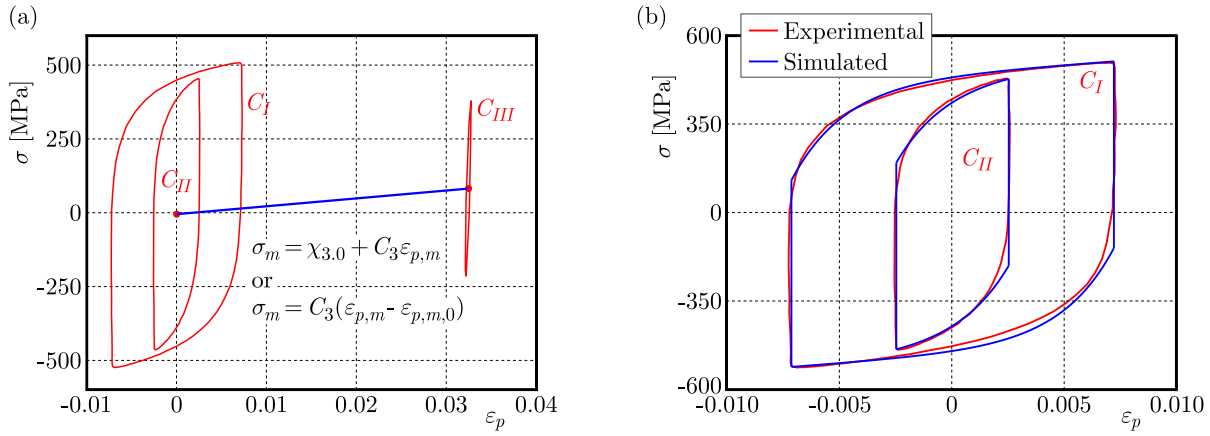

Fig. 5. (a) Average points of the stabilized cycles of the SCTs, (b) small differences between experimental and reproduced C_I and C_{II} cycles by using the proposed procedure with three backstress components

The ratcheting rate was also modelled, and the obtained results are reported in Fig. 6. The comparison between the experimental and the modelled ratcheting rates is reported in Fig. 6a. Clearly, this latter comparison was carried out in the region where the ratcheting rate could be considered constant according to Fig. 2. In Fig. 6b, a comparison between the experimental and the modelled FCT is shown in the same ratcheting cycle range.

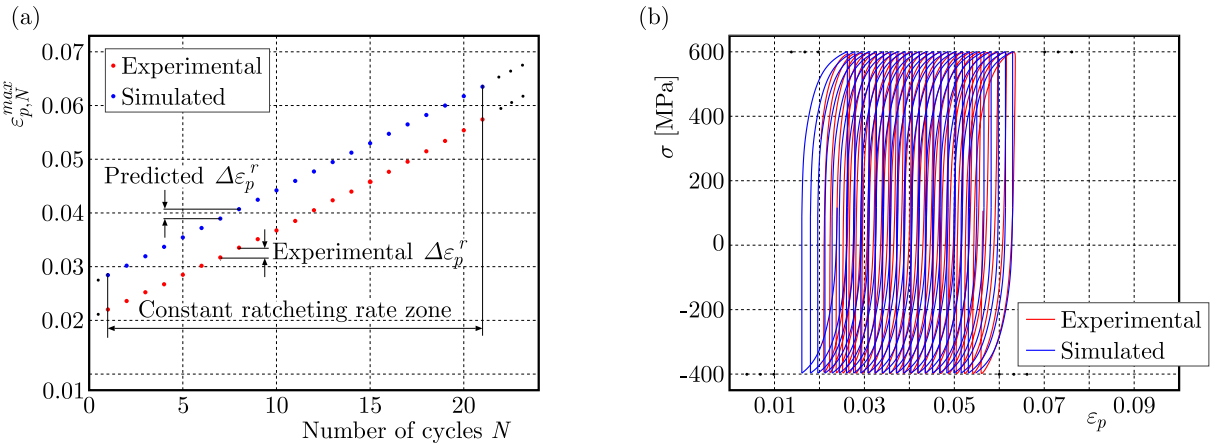

Fig. 6. (a) Differences between experimental and modelled ratcheting rates in the constant ratcheting rate region and (b) differences among experimental and modelled fully reproduced cycles of the force-controlled test in the same constant ratcheting region

The fourth backstress, with an imposed high value of γ_4, thus quickly saturating, was added to improve the prediction of the stabilized cycles of the SCTs near the elastic limit region. The searched ratio between C_4 and γ_4 was aimed at minimizing the further error function described by

$$\varphi\left(\frac{C_4}{\gamma_4}\right) = |\sigma_A - \sigma_B|^2 + |\sigma_C - \sigma_D|^2 \tag{3.11}$$

A graphical and qualitative explanation of the error function described by this latter equation is provided in Fig. 7a. The superimposition of the fourth backstress, with a high value of γ_4, modifies Eqs. (3.4). In fact, the elastic limit can be modelled as $\sigma'_L = \sigma_L - C_4/\gamma_4$, where σ'_L is the updated (and lower) value of the elastic limit provided that σ_L is the value of the elastic limit previously obtained with the CKH model with three backstress components. The updated expression of the elastic limit can be then substituted into Eqs. (3.5) leading to a clear decrease in the value of the modelled HA. Finally, the comparisons between the experimental and simulated stabilized cycles, considering the fourth backstress component and for C_I, C_{II} and C_{III}, are reported in Fig. 7b. The numerical values of the obtained CKH parameters are shown in Table 2.

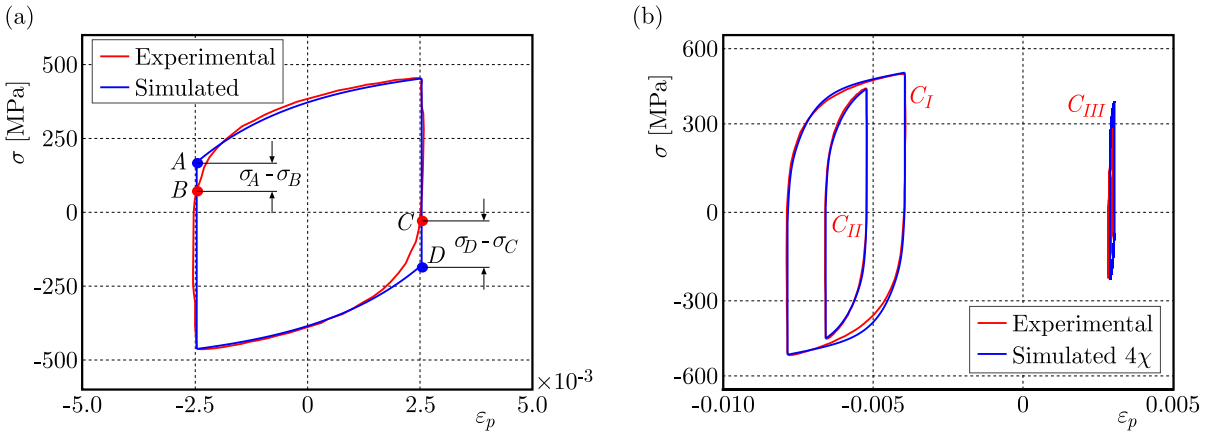

Fig. 7. (a) Inaccuracy of the simulated stabilized cycle, which can be corrected by introducing the fourth backstress component, (b) differences among experimental and modelled C_I, C_{II} and C_{III} considering the additional fourth backstress component

Table 2. Obtained parameters for the CKH model with four backstress components

σ_L [MPa	C_1 [MPa]	γ_1 [–]	C_2 [MPa]	γ_2 [–]	C_3 [MPa]	γ_3 [–]	$\chi_{3,0}$ [MPa]	C_4 [MPa]	γ_4 [–]
240	69200	426	2840	4.63	2670	0	−4.86	38200	5000

4. Use of the Bouc-Wen model to describe the cyclic-plastic behaviour

The B-W model is widely used to describe the hysteretic behaviour of mechanical systems, and its general form is described as

$$\begin{aligned} &Y = Y_2(z + Y_1) \qquad Y_1 = k_1 x + k_2 \operatorname{sgn}(x) x^2 + k_3 x^3 \qquad Y_2 = b^{cx} \\ &\dot{z} = \dot{x}\Big(\alpha + \delta x - [\gamma + \beta \operatorname{sgn}(\dot{x}) \operatorname{sgn}(z)] z^n\Big) \end{aligned} \tag{4.1}$$

In these equations, the variable x and its derivative with respect to time $\dot{x}$ are the input variables, while Y is the output variable. It is important to highlight, by considering the last expression of Eqs. (4.1), that the time variable could be simplified, thus leading to a not time-dependent expression. However, the time variable defines the sequence of the loading, i.e. the change of sign of the input variable x, but the velocity of change of this variable does not affect the output of the problem. As a consequence, in all performed searches of the Bouc-Wen model parameters presented below, the time was never involved. In the last equation of Eqs. (4.1), the term δx was added with respect to the original formulation of the model, as in (Neri and Holzabuer,

2023). This added term aims to reproduce the possible asymmetry between the two EPOC. In this research, the input variables were the axial plastic strain ε_p and its differential $d\varepsilon_p$, while the output variable Y represented the axial stress. The parameters of the B-W model were calculated by the Levenberg-Marquardt algorithm. This algorithm combines the steepest--descent and the Newton-Raphson methods, thus obtaining two different types of behaviour: far from possible singularities, the algorithm tends to enhance Newton-Raphson to improve the convergence rate, while, in order to improve its robustness, it tends to the steepest-descent algorithm near eventual singularities to improve its robustness. This latter characteristic can then balance between the aim of convergence and the robustness to the singularities. The Levenberg--Marquardt algorithm is fully implemented in the MATLAB software, which is widely employed in optimization problems. The results of this algorithm are presented in Fig. 8. The parameters were firstly calibrated by C_I and validated by C_{II} (Fig. 8a) and vice versa (Fig. 8b). The parameters were also calculated for the FCT, as shown in Fig. 9. The obtained B-W parameters are reported in Table 3.

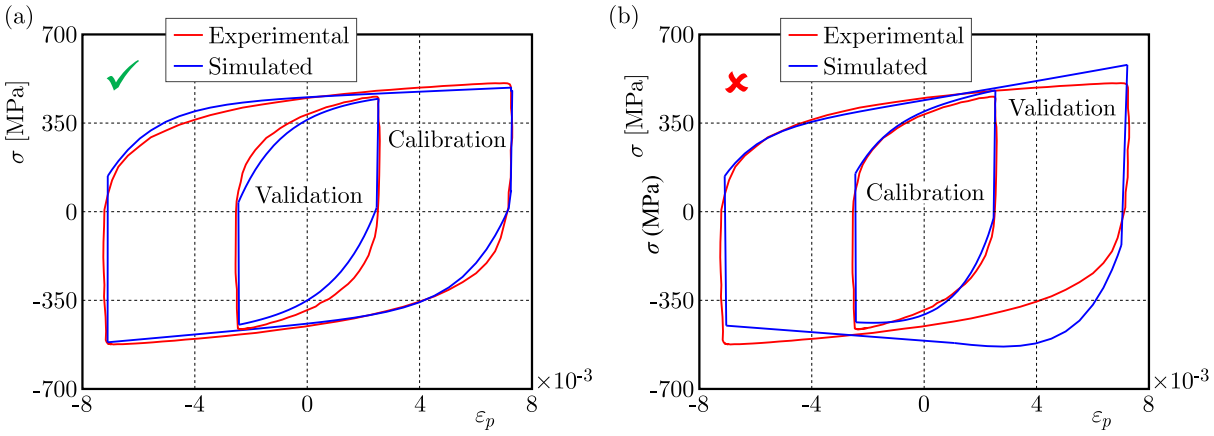

Fig. 8. Differences among experimental and simulated C_I and C_{II} by involving the B-W model: (a) C_I employed to calculate the constants of the B-W model and C_{II} utilized to validate the obtained constants, (b) C_{II} employed to calculate the constants of the B-W model and C_I utilized to validate the obtained constants. This latter approach introduces higher errors

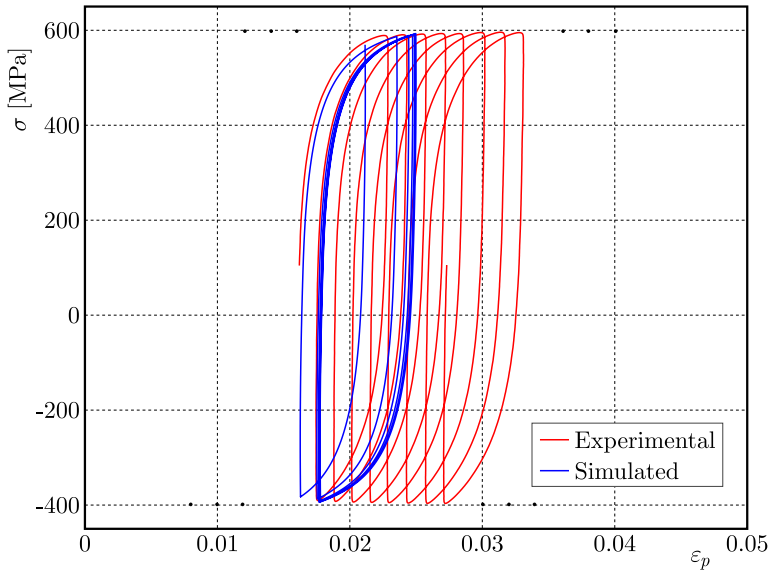

Fig. 9. Comparison between the experimental and the predicted force-controlled test by using the Bouc-Wen model

Table 3. Calculated constants of the B-W model

Extracted from	α [MPa]	β [MPa^{1-n}]	γ [MPa^{1-n}]	n	δ [MPa]	c	k_1 [MPa]	k_2 [MPa]	k_3 [MPa]
C_I	28.7	14.8	−13.7	0.860	−0.139	0	0.738	0	0
C_{II}	40.6	37.7	−34.8	0.681	1.12	0	0	0	0
Force--controlled test	15.5	0.068	0.036	1.290	−0.026	0	0.479	0	0

After critically considering the obtained values of the B-W parameters reported in Table 3, it can be observed that this model collapses for all the investigated cases into equations (4.2), given that from the optimization algorithm it was found out that $k_2 = k_3 = c = 0$, $\delta \approx 0$ and $n \approx 1$. A null value of k_1 was identified only when the optimization was carried out on C_{II}, while it was considerably not null in the other cases. According to Eqs. (4.2), the output variable Y was obtained by the sum of z and Y_1, which resemble nonlinear and linear backstress components, respectively. Therefore, under these circumstances, the B-W model collapsed into the CKH model with two backstress components in which one was nonlinear and the other was linear. In addition to this, the term $\gamma + \operatorname{sgn}(x)\operatorname{sgn}(z)$, which is the equivalent of γ of in the CKH model, varies during the loading due to the sign of x and sign of z, while γ in the CKH model remains constant during the loadings

$$\begin{aligned} &Y = z + Y_1 \qquad Y_1 = k_1 x \qquad Y_2 = 1 \\ &dz = dx\Big(\alpha - [\gamma + \beta \operatorname{sgn}(dx)\operatorname{sgn}(z)]z\Big) \end{aligned} \tag{4.2}$$

5. Conclusions

In this research, the cyclic-plastic behaviour of plain specimens made of 42CrMo4 (Q+T) was analyzed with the Chaboche kinematic hardening model and, for a comparative purpose, also with the Bouc-Wen model. The main findings of this research are reported below:

- The employed novel procedure to identify the Chaboche kinematic hardening model parameters is based on the global properties, such as the gradient at the EPOC, the HA, the AS, the SR, the PSR and the APS of the stabilized cycles obtained from the SCTs and on the ratcheting rate obtained from the FCT.
- The parameters of the Chaboche kinematic hardening model with three backstress components were tuned, and the fourth backstress was eventually added to improve the prediction accuracy near the elastic limit regions. The procedure allowed one to obtain a good prediction accuracy as highlighted in Fig. 5 for the Chaboche model with three backstress components, in Fig. 6 for the ratcheting rate and in Fig. 7 for the Chaboche model with four backstress components. In this latter figure, C_{III} was used as an independent validator given that it was only employed to calculate the values of C_3 and $\chi_{3,0}$. The utilized procedure makes use only of explicit formulas, and it avoids the use of complex optimization algorithms.
- Given that cyclic plasticity introduces a hysteretic phenomenon, the Bouc-Wen model was also engaged to reproduce the cyclic-plastic behaviour of the investigated steel. The Bouc--Wen parameters were tuned by C_I and validated by C_{II} and vice versa. For comparison, the parameters were also calculated from the FCT. In Fig. 8, it is shown that the Bouc--Wen model can accurately reproduce the stabilized cycle from which the parameters were obtained, but a lack of accuracy was observed when they were employed to reproduce

the stabilized cycle of the SCT not accounted for calibration. More precisely, the model if calibrated by C_I and validated by C_{II}, see Fig. 8a, provided a better prediction accuracy than in, vice versa, Fig. 8b. This latter behaviour can be explained just considering that the strain range of C_I was wider than that of C_{II}.

- By observing the obtained numerical results for the Bouc-Wen parameters reported in Table 3, it can be noted that this model collapsed for the investigated data into something very similar to the Chaboche kinematic hardening model with nonlinear and linear backstress components. It is reasonable to obtain $k_2 = k_3 = 0$, given that these two parameters can change the sign of concavity of the quantity Y during the tensile loading phase or during the compressive loading phase, as shown in (Neri and Holzbauer, 2023). This mentioned change of concavity makes no sense if contextualized for cyclic-plastic phenomena where the concavity has a positive sign during the entire compressive loading phase, and it has a negative sign during the entire tensile loading phase. It is also reasonable to obtain a low value of δ, if compared to the obtained value of α, given that generally there is not an evident asymmetry between the two EPOC in the cyclic plastic behaviour. However, rather than the Chaboche, the Bouc-Wen model misses the equivalent of the term σ_L, which allows one to model the elastic limit stress of the material.
- The Bouc-Wen model did not provide an accurate description of the ratcheting rate even if the model parameters search were optimized in a force-controlled test, as shown in Fig. 9. As explained in (Santus *et al.*, 2023a), the relationship between the SR and the PSA per cycle $\Delta\varepsilon_p^a$ in a force-controlled test is equal to the relationship between the SR and the PSA for a stabilized cycle obtained from a SCT test (Eqs. (3.4)). During determination of the Chaboche model parameters, according to our procedure, the SCTs are primarily employed to calculate the parameters and then the FCT is employed to calculate just the value of γ_2 of the slightly nonlinear backstress component. Following this approach, when calculating the value of γ_2, the relationship between the SR and the PSA per cycle is generally satisfied due to the previous tuning of the backstress with the most rapid dynamics. Reconsidering the equivalent CKH model, if only a slightly nonlinear backstress component is employed, Eq. (3.8) can be used to calculate the value of γ_2, but Eqs. (3.4) cannot be satisfied in general, since another nonlinear backstress component is required to provide an accurate reproduction of the FCT.

Acknowledgement

This paper was presented at WECM'23 – 2nd Workshop on Experimental and Computational Mechanics (Pisa, Italy, 20-22 September, 2023). Based on the evaluation by Selection Committee chaired by Prof. Jerzy Warmiński, Lublin University of Technology, Poland, and composed of Prof. Simone Camarri and Prof. Luigi Lazzeri, University of Pisa, Italy, this work was awarded the "WECM'23 Best Paper Award in Experimental Mechanics". Authors gratefully acknowledge the University of Pisa for the organisation of the workshop and for the payment of the publication fee.

References

1. Badnava H., Pezeshki S.M., Fallah Nejad K., Farhoudi H.R., 2012, Determination of combined hardening material parameters under strain controlled cyclic loading by using the genetic algorithm method, *Journal of Mechanical Science and Technology*, **26**, 3067-3072

2. Bertini L., Le Bone L., Santus C., Chiesi F., Tognarelli L., 2017, High load ratio fatigue strength and mean stress evolution of quenched and tempered 42CrMo4 Steel, *Journal of Materials Engineering and Performance*, **26**, 3784-3793

3. Bouc R., 1967, Forced vibrations of mechanical systems with hysteresis, *Proceedings of the Fourth Conference on Nonlinear Oscillations*, Prague, Czech Republic, **10**, 142-149
4. Cai J., Dong W., Nagamune R., 2023, A survey of Bouc-Wen hysteretic models applied to piezo-actuated mechanical systems: Modeling, identification, and control, *Journal of Intelligent Material Systems and Structures*, **34**, 16, 1843-1863
5. Chaboche J.L., 1986, Time-independent constitutive theories for cyclic plasticity. *International Journal of Plasticity*, **2**, 149-188
6. Chaboche J.L., 1991, On some modifications of kinematic hardening to improve the description of ratchetting effects, *International Journal of Plasticity*, **7**, 661-678
7. Chaparro B.M., Thuillier S., Menezes L.F., Manach P.Y., Fernandes J.V., 2008, Material parameters identification: Gradient-based, genetic and hybrid optimization algorithms, *Computational Materials Science*, **44**, 339-346
8. Charalampakis A.E., Dimou C.K., 2010, Identification of Bouc-Wen hysteretic systems using particle swarm optimization, *Computers and Structures*, **88**, 21-22
9. Dafalias Y.F., Kourousis K.I., Saridis G.J., 2008, Multiplicative AF kinematic hardening in plasticity, *International Journal of Solids and Structures*, **45**, 2861-2880
10. Dvoršek N., Stopeinig I., Klančnik S., 2023, Optimization of Chaboche material parameters with a genetic algorithm, *Materials*, **16**, 1821
11. Hosseini R, Seifi R., 2020, Fatigue crack growth determination based on cyclic plastic zone and cyclic J-integral in kinematic–isotropic hardening materials with considering Chaboche model, *Fatigue and Fracture of Engineering Materials and Structures*, **43**, 2668-2682
12. Karolczuk A, Skibicki D, Pejkowski Ł., 2019, Evaluation of the Fatemi-Socie damage parameter for the fatigue life calculation with application of the Chaboche plasticity model, *Fatigue and Fracture of Engineering Materials and Structures*, **42**, 197-208
13. Koo G.-H., Lee J.-H., 2007, Investigation of ratcheting characteristics of modified 9Cr-1Mo steel by using the Chaboche constitutive model, *International Journal of Pressure Vessels and Piping*, **84**, 284-292
14. Kreethi R., Mondal A.K., Dutta K., 2017, Ratcheting fatigue behaviour of 42CrMo4 steel under different heat treatment conditions, *Materials Science and Engineering*, **679**, 66-74
15. Li J., Li Q., Jiang J., Dai J., 2018, Particle swarm optimization procedure in determining parameters in Chaboche kinematic hardening model to assess ratcheting under uniaxial and biaxial loading cycles, *Fatigue and Fracture of Engineering Materials and Structures*, **41**, 1637-1645
16. Mahmoudi A.H., Badnava H., Pezeshki-Najafabadi S.M., 2011, An application of Chaboche model to predict uniaxial and multiaxial ratcheting, *Procedia Engineering*, **10**, 1924-1929
17. Neri P., Holzbauer J., 2023, Experimental characterization and numerical modeling of wire rope isolators, *Proceedings of the Nodycon: Third International Nonlinear Dynamics Conference*, Rome, Italy
18. Ni Y.Q., Ko J.M., Wong C.W., 1998, Identification of non-linear hysteretic isolators from periodic vibration tests, *Journal of Sound and Vibration*, **217**, 737-756
19. Ortiz G.A., Alvarez D.A., Bedoya-Ruíz D., 2013, Identification of Bouc-Wen type models using multi-objective optimization algorithms, *Computers and Structures*, **114-115**, 121-132
20. Santus C., Grossi T., Romanelli L., Pedranz M., Benedetti M., 2023a, A computationally fast and accurate procedure for the identification of the Chaboche isotropic-kinematic hardening model parameters based on strain-controlled cycles and asymptotic ratcheting rate, *International Journal of Plasticity*, **160**, 103503
21. Santus C., Romanelli L., Grossi T., Neri P., Romoli L., *et al.*, 2022, Torsional-loaded notched specimen fatigue strength prediction based on mode I and mode III critical distances and fracture surface investigations with a 3D optical profilometer, *International Journal of Fatigue*, **161**, 106913

22. Santus C., Romanelli L., Grossi T., Bertini L., Le Bone L., *et al.*, 2023b, Elastic-plastic analysis of high load ratio fatigue tests on a shot-peened quenched and tempered steel, combining the Chaboche model and the Theory of Critical Distances, *International Journal of Fatigue*, **174**, 107713

23. Shafiqul B., Tasnim H., 2000, Anatomy of coupled constitutive models for ratcheting simulation, *International Journal of Plasticity*, **16**, 381-409

24. Wen Y.K., 1976, Method for random vibration of hysteretic systems, *Journal of Engineering Mechanics, ASCE*, **102**, 249-263

25. Zhang B., Wang R., Hu D., Jiang K., Hao X., *et al.*, 2020, Constitutive modelling of ratcheting behaviour for nickel-based single crystal superalloy under thermomechanical fatigue loading considering microstructure evolution, *International Journal of Fatigue*, **139**, 105786

Manuscript received November 22, 2023; accepted for print January 13, 2024